PRODUCTION OF SYNGAS BY ETHANOL REFORMING ON Ni CATALYST

Rafael C. Catapan, catapan@labcet.ufsc.br
Amir. A. M. Oliveira, amir.oliveira@gmail.com
Laboratory of Combustion and Thermal Systems Engineering
Department of Mechanical Engineering, Federal University of Santa Catarina - Campus Universitário João David Ferreira Lima, Florianópolis - SC – Brazil, 88040-900

Karina Donadel, donadel@emc.ufsc.br
Antonio Pedro N. Oliveira, pedronovaes@emc.ufsc.br
Carlos R. Rambo, rambo@enq.ufsc.br
Group of Ceramic and Glass Materials
Department of Mechanical Engineering, Federal University of Santa Catarina - Campus Universitário João David Ferreira Lima, Florianópolis - SC – Brazil, 88040-900

Therezinha Maria N. Oliveira, tnovais@univille.br
Theodoro M. Wagner, theowag@terra.com.br
Universidade da Região de Joinville
Campus Universitário, Bom Retiro
Joinville - SC – Brazil, 89201-972

Abstract. *In the recent literature, attention has been directed to the development of noble metals based catalysts for the ethanol reforming. However, the high costs and low availability of noble metals, e.g. platinum, as a resource justify the development of alternatives technologically, economically and environmentally viable such as Ni-based catalysts. Here, the thermal decomposition, partial oxidation and steam reforming of ethanol over SiO_2 supported Ni was studied in a packed bed reactor in the 673 - 973 K temperature range at 1 atm. The catalyst was produced from 10% NiO, 5% of bentonite and 85% (wt.) of natural amorphous silica fibers (NASF). Scanning Electron Microscopy (SEM) evaluation revealed that particles of Ni were homogeneously distributed over the NASF. The X-ray diffraction (XRD) patterns did not show peaks related to silicates in all spectra, which indicates that there is no, apparenly, interaction between the nickel catalysts and SiO_2 or devitrivication The reactions of ethanol on this catalyst occurs mainly by the dehydrogenation reaction generating acetaldehyde. Further, CH_3CHO is decomposed to CH_4 and CO. In parallel to this route, ethanol is dehydrated producing ethylene, which is successively dehydrogenated in Ni sites generating carbon on the surface. Also, carbon can be produced by consecutive dehydrogenation of CH_4. Both reactions contribute to increase the production of H_2 to values higher than those predicted by the thermodynamic equilibrium.*

Keywords*: ethanol, syngas, Ni catalyst, ceramic filters, renewable energy*

1. INTRODUCTION.

The development of technologies based on renewable energy sources has received great attention around the world due to the current drive to decreases the emission of greenhouse gases and to attain energy security. Brazil has a peculiar position in the world scenario due to its large-scale use of ethanol exclusively as an automotive fuel, displacing gasoline, making use of a well established structure for production, storage and transportation. All this structure allows the development of new technologies for the use of ethanol in others sectors of the economy. Some innovative, but not yet commercially available alternative to use ethanol include the local generation of electricity by using an internal high temperature reformer coupled with either Solid Oxide Fuel Cells (SOFC) or Molten Carbonate Fuel Cells (MCFCs) or the generation of a H_2-rich syngas to be used in industries as a source of chemicals or gaseous fuel in heating processes.

For both alternatives, the most feasible route nowadays is to promote the syngas production at a catalytic reactor prior to feeding it to the process itself. This calls for highly efficient, effective and low cost reformers and catalysts. In the recent literature, attention has been directed to the development of noble metals based catalysts for the ethanol reforming due to their high activity and good selectivity to H_2 mainly for use in direct ethanol fuel cells [Alcalá et al., 2003; Vesselli et al., 2005; Lima et al., 2008; Silva et al., 2008]. However, the high costs and low availability of noble metals, e.g. platinum, as a resource justify the development of alternatives technologically, economically and environmentally viable. One of them is the use of Ni-based catalysts. Nickel is widely used in the petrochemical industries for steam reforming of natural gas. Although its activity is lower than that of noble metals, promising results have been obtained in the thermal decomposition [Gates et al., 1986; Wang et al., 2009], partial oxidation and steam reforming of ethanol [Liberatori et al., 2007]. In this class of catalysts, the deactivation due to surface deposition of carbon is still a great challenge.

In this context, the main objective of this work is to evaluate the production of syngas from reforming of ethanol in filters produced from natural amorphous silica fibers (NASF) as a support coated with Ni (catalyst). The manufacturing process as well as the characterization of the catalyst are addressed. The results are discussed in order to clarify the

main steps of the reaction mechanism that represent the process. The influence of the support on the by-products is also discussed.

2. EXPERIMENTAL METHODS

The catalyst used was made from 85% of natural amorphous silica fibers (NASF) as a support, 5% of bentonite and NiO 10 wt%. By convenience, we use NASF to refer only to support ans Ni/NASF to refer to the catalyst during the text. The mixture was humidified and pressed uniaxially pressed at 3.5 MPa. Then, the samples were reduced under an atmosphere of 5% H_2/95% N_2 at 773 K for 1h, with subsequent sintering in an inert atmosphere at 1273 K for 1h (Donadel, 2010). The final product of such procedure is a cylindrical pellet with 30 mm diameter and 10 mm length. The desired particle diameter was produced by crushing the sample and passing through sieves (60-140 mesh). Powder X-ray diffraction (XRD - Philips, X´Pert) with CuKα radiation was used to identify the phases of the catalyst. Morphology and microstructure of the catalyst were evaluated by scanning electron microscopy, (SEM - XL-30, Philips). Pore diameter and nickel particle diameter were identified using image analysis (IMAGO). Other characterizations include standard techniques for Ni content (ICM-MS), BET area and porosity.

Thermal decomposition, partial oxidation and steam reforming reactions were carried out in an atmospheric-pressure packed bed reactor. Figure 1 shows scheme of the experimental apparatus used in this work. The reactor consists of a 4 mm diameter quartz tube placed inside an electric furnace. The temperature of the furnace was kept constant by aid of a controller, which includes a type K thermocouple placed close to the reactor. For each new run, the reactor was filled with 300 mg of catalyst with particle diameter between 100 and 250 µm, which correspond to a 40 mm packing in the reactor. Ethanol and water were fed to the reactor by a steady flow of N_2 (N50, 99.999% pure) passing through a bubble saturator filled with either ethanol (P.A. 99.8% pure) or a water/ethanol mixture in the desired ratio. Oxygen was fed from a bottle of synthetic air (20% O_2/N_2 – P.A. 99.95%). Calibrated orifice plates interfaced to a micro-manometer were used to measure the volumetric flow rate of N_2 and synthetic air. Table 1 presents the experimental conditions in which the tests were carried out.

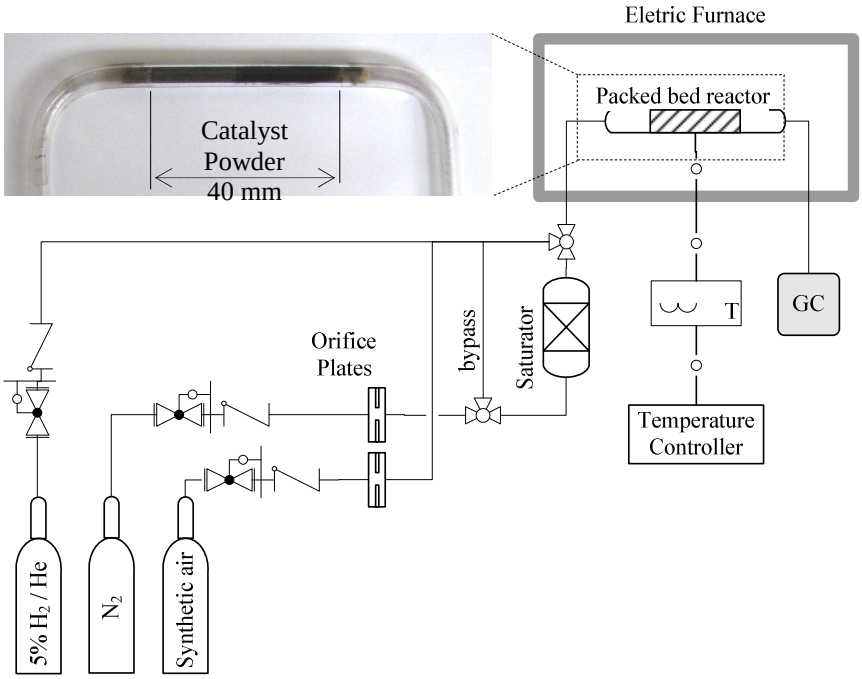

Figure 1. Experimental apparatus.

Table 1. Experimental conditions.

Reaction	*Molar composition* [C_2H_5OH:H_2O:O_2]	*Total volumetric flow rate* [cm^3/min]	*N_2 dilution* [%]	*Space time* [g_{Ni}.s/$cm^3_{ethanol}$]
Thermal decomposition – TD	1 : 0 : 0	108	92%	0.16
Partial oxidation - POX	1 : 0 : 0.52	115	87%	0.13
Steam reforming - SR	1 : 0.68 : 0	108	92%	0.24

Before each measurement, the catalyst was reduced *in-situ* at 773 K during 40 minutes by a flow of 5% H_2/He (50 cm^3/min). Then, the reactor was cooled down or heated up until the desired temperature under a flow of N_2. This process takes 20 minutes. The furnace was kept under the reaction temperature by at least 20 minutes to avoid temperature gradients in the reactor. The reactants were supplied in the reactor 10 minutes before the sampling. The samples were collected in glass ampoules and injected manually in a gas chromatography (Agilent - 6980) equipped with a thermal conductivity detector. To separate all the species found in the products, two runs were carried out. First, a molecular sieve 5A capillary column (Agilent 19091P-MS4 – 30 m, 0.32 mm and 12 μm) was used to separate permanent gases like H_2, O_2, N_2 and CO. Then, a new run was carried out in a Poraplot Q capillary column (Agilent 19091P-Q02 – 30 m, 0.32 mm and 20 μm) to separate CH_4, CO_2, C_2H_4, C_2H_6, CH_3CHO and C_2H_5OH. Helium was used as carrier gas in all runs.

The absence of internal mass transfer limitation was verified by the Weisz-Prater criterion, which requires that $(r'_A\rho_c R_p)/(D_e C_{A,s}) \ll 1$. For the reaction temperature of 923 K, the measured reaction rate (r'_A) was $1.722\cdot10^{2}$ mol/kg.s. The effective diffusivity of C_2H_5OH in the catalyst pellet is defined as $D_e = D_{C2H5OH\text{-}N2}\varepsilon_p\sigma/\tau$, where typical values for the diffusion coefficient of C_2H_5OH in N_2 $D_{C2H5OH\text{-}N2} = 1.8\cdot10^{-5}$ m^2/s, for the constriction factor $\sigma = 0.8$ and for the tortuosity $\tau = 3$ were used. The other parameters are the catalyst density $\rho_c = 878$ kg/m^3, the pellet porosity $\varepsilon_p = 0.63$, the pellet radius $R_p = 1.75\cdot10^{-4}$ m and the C_2H_5OH concentration at the pellet surface $C_{A,s} = 1.13$ mol/m^3, which was taken as equal to the bulk concentration. The Weisz-Prater criterion results in $3.3\cdot10^{-2}$.

The Mears`criterion, which requires that $r'_A(1-\varepsilon_p)\rho_c R_p n/(k_c C_{A,b}) < 0.05$, was applied to investigate the limitation by external mass transfer. The mass transfer coefficient (k_c) was estimated from the Sherwood's number (Sh) calculated from the Frössling's correlation defined as $Sh = 2 + 0.6Re^{0.5}Sc^{0.33}$, where the Reynolds'number (Re) is based on the pore diameter and Sc is the Schimidt's number. Here, in the absence of a better estimative, a conservative value was taken to the reaction order n = 2. The Mears'criterion results in 0.002.

3. RESULTS AND DISCUSSIONS.

3.1. Catalyst characterization

Scanning Electron Microscopy (SEM) evaluation revealed that particles of Ni were homogeneously distributed over the NASF (Fig. 2). The powder XRD patterns for Ni/NASF before and after reduction are shown in Fig. 3. SiO_2 exists as an amorphous phase since that any silica crystalline phase was formed. The peaks at $2\theta = 37^o$, 43^o, 63^o, 75^o and 79^o are characteristic of NiO (ICDD PDF card 04-835) before reduction. The XRD patterns of the catalyst after reduction process under a 5% H_2/95% N_2 shows peaks at $2\theta = 44^o$, 52^o, 76^o that are assigned to metallic nickel (ICDD PDF card 04-850) evidencing the reduction of the NiO. The absence of the peaks attributed to silicates in all spectra indicates that there is no, apparently, interaction between the nickel and the NASF. Table 2 shows the main physical and chemical properties of the NASF and Ni/NASF used in the present work.

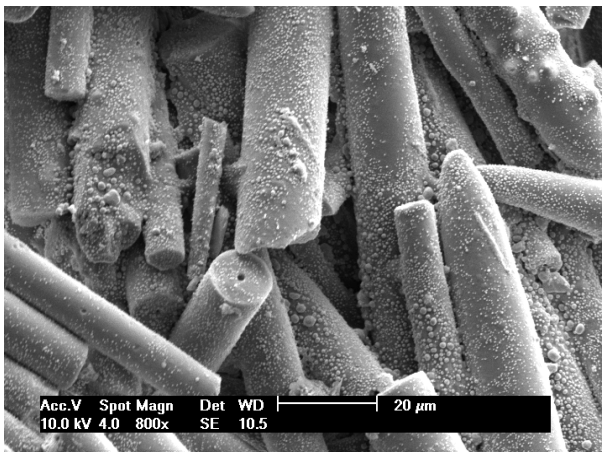

Figure 2. SEM micrographs of Ni/NASF catalyst.

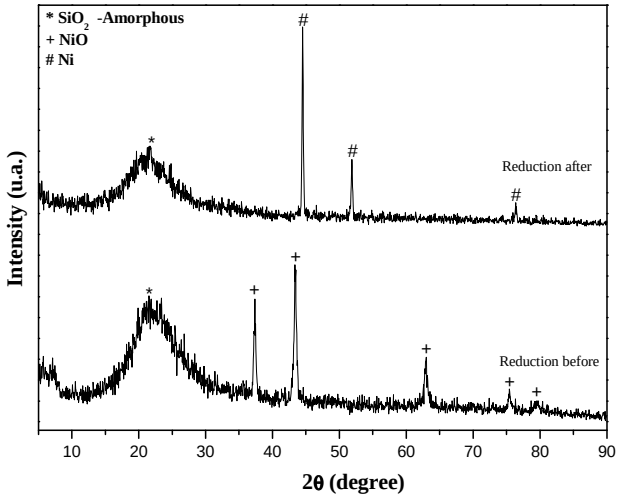

Figure 3. XRD patterns of Ni/NASF before and after reduction.

Table 2. Properties of the catalysts.

Catalyst	*Ni content after reduction* [wt%]	*Specific surface area* [m^2/g]	*Porosity* [%]	*Pore diameter* [µm]	*Ni particle diameter* [µm]
NASF	0	< 0.01	63.9	20.1	-
Ni/NASF	6.8	11.1	63.9	23.1	0.17

3.2 Effect of the support on the reaction pathway

Figure 4 presents the mole fraction of the C_2 species measured from TD of ethanol (a) on Ni/NASF and (b) on NASF. TD results are preferable to be presented here instead of other reactions conditions since the results are further from the thermodynamic equilibrium than POX and SR reactions at low temperatures on Ni/NASF and in all range of temperatures studied for reaction on NASF.

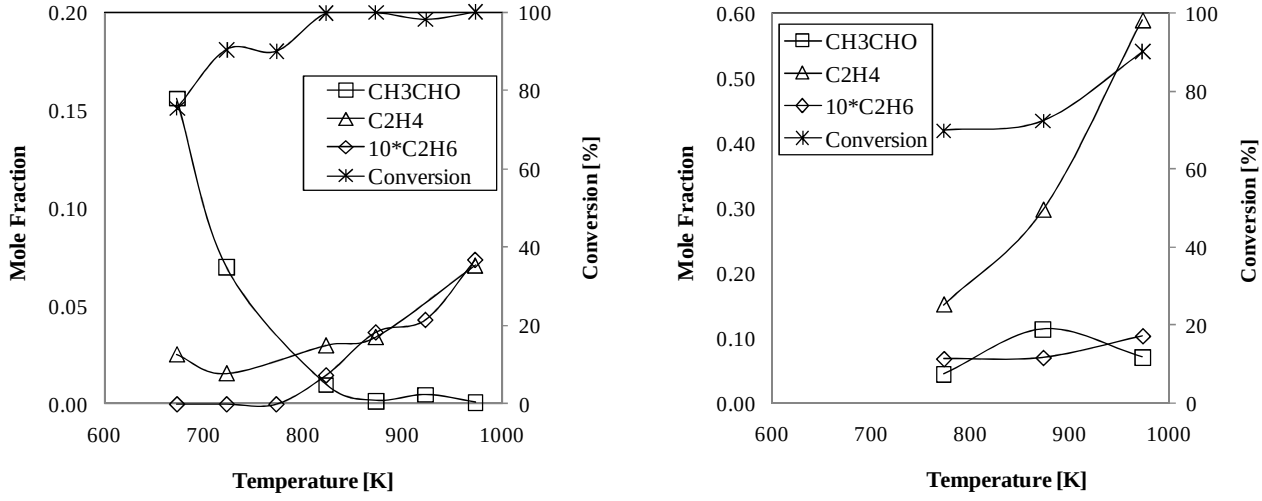

(a) (b)

Figure 4. Gas phase mole fraction of C_2 species from thermal decomposition (TD) of ethanol on (a) Ni/NASF and (b) NASF. Experimental conditions are presented in the Table 1.

The conversion of ethanol was high in both cases, with values above 90% for temperatures higher than 823 K on Ni/NASF. For 673K (Fig. 4a) and below 873K (Fig. 4b) the conversion of ethanol calculated was lower than 80%. However, the mass balance for the elements H and O resulted in differences between reactants and products of about 60%, while the differences are in general less than 10% for higher temperatures. We attribute this discrepancy to the intrinsic difficult of the sampling process, which allowed the condensation of saturated species such as ethanol on the glass ampoules, decreasing their concentration in gas phase.

The TD of ethanol occurs mainly by the dehydrogenation reaction (R.1) generating acetaldehyde. Further, CH_3CHO is decomposed to CH_4 and CO (R.2). This pathway is evidenced by CH_4/CO molar ratio close to 1 at 673 K (see Fig. 5a). Such pathway is also observed by TPD of ethanol on Ni 111 surface [Gates et al., 1986] and from steam reforming on Ni/Al_2O_3-La [Liberatori et al., 2007]. Mavrikakis and Barteau (1998) show evidences that this is the main route for ethanol decomposition on transition metals of the VIIIB group.

Another important pathway in the ethanol decomposition evidenced by the experimental results is the dehydration reaction (R.3) producing ethylene. Such route is undesired in the production of syngas since C_2H_4 is known as a precursor of soot, which poisons the catalysts speeding up its deactivation. The C_2H_4 is successively dehydrogenated in Ni sites generating carbon in an irreversible reaction (R.4). Also, carbon can be produced by consecutive dehydrogenation of CH_4 through reaction R.5. Both reactions contribute to increase the production of H_2 to values higher than those predicted by the thermodynamic equilibrium (see Fig. 5a).

From the literature, we could not find evidences about the production of C_2H_4 from thermal decomposition of ethanol on Ni. The production of C_2H_4 is common on acid sites such as those of γ-Al_2O_3 at high temperatures [Liberatori et al., 2007; Wang et al., 2009]. Therefore, we attribute the presence of C_2H_4 as caused by reaction on the support. The results in Fig. 4b show that the main by-product is C_2H_4 mainly at high temperature. Futhermore, hydrogenolysis of C_2H_4 occurs in a fraction of the C_2H_4 produced (R.6) at high temperature, generating ethane in a level one order of magnitude lower than other C_2 products in both catalyst Ni/NASF and NASF.

$$C_2H_5OH = CH_3CHO + H_2 \quad \text{R.1}$$
$$CH_3CHO = CH_4 + CO \quad \text{R.2}$$
$$C_2H_5OH = C_2H_4 + H_2O \text{ on the support} \quad \text{R.3}$$
$$C_2H_4 => 2C + 2H_2 \quad \text{R.4}$$
$$CH_4 => C + 2H_2 \quad \text{R.5}$$
$$C_2H_4 + H_2 = C_2H_6\,. \quad \text{R.6}$$
$$CH_4 + H_2O = CO + 3H_2 \quad \text{R.7}$$
$$CH_4 + CO_2 = 2CO + 2H_2 \quad \text{R.8}$$
$$CO + 0.5O_2 = CO_2 \quad \text{R.9}$$
$$C + 0.5O_2 = CO \quad \text{R.10}$$

3.3 Syngas production

Figure 5 presents the gas phase mole fraction for CH_4, H_2, CO and CO_2 produced by (a) TD, (b) POX and (c) SR of ethanol on Ni/NASF catalyst. The experimental conditions are presented in the Table 1. Additionally, Fig. 5 presents the gas phase mole fraction predicted by the thermodynamic equilibrium. The software Stanjan [Reynolds, 1986] was used utilizing the same species listed in the Marinov mechanism for high temperature ethanol oxidation [Marinov, 1988] with the thermochemical properties based on the Burcat and Ruscic's work [Burcat and Ruscic, 2005].

For TD reaction at low temperature range (Fig. 5a), syngas is produced mainly by reaction R.1 and R.2. Also, H_2 presents a mole fraction always higher than the predicted by the equilibrium conditions, evidencing the presence of both R.4 and R.5 irreversible reactions in all range of temperature. The high level of H_2 displaces the equilibrium of the steam reforming reaction (R.7), decreasing the CO concentration as measured in the high temperature range. The excess of CH_4 produced is consumed in either reaction R.5 or in the dry reforming reaction (R.8) which explains the low level of CO_2 measured.

The presence of the O_2 in the feed in the POX reaction (Fig. 5b) contributed to increase substantially the reaction rate, making the by-products composition close to equilibrium even for low temperature. Only CO oxidation reaction (R.9) is not equilibrated at low temperature range since the conversion of O_2 is not 100% in such region. At high temperature range the reverse of the steam reforming reaction favored (R.7), increasing the CH_4 mole fraction. Also, the production of C_2H_4 and C_2H_6 is favored at high temperature for both POX and SR reactions. Since CH_4 is almost equilibrated in most part of the temperature range, a lower catalyst deactivation of the POX reaction is expected. Additionally, surface carbon can be substantially removed by oxygen (R.10). For the SR reaction at the experimental conditions presented here, the mole fractions of the main constituents of the syngas are close to the thermodynamic equilibrium. Only for low temperature the oxidation of CO (R.9) is not equilibrated.

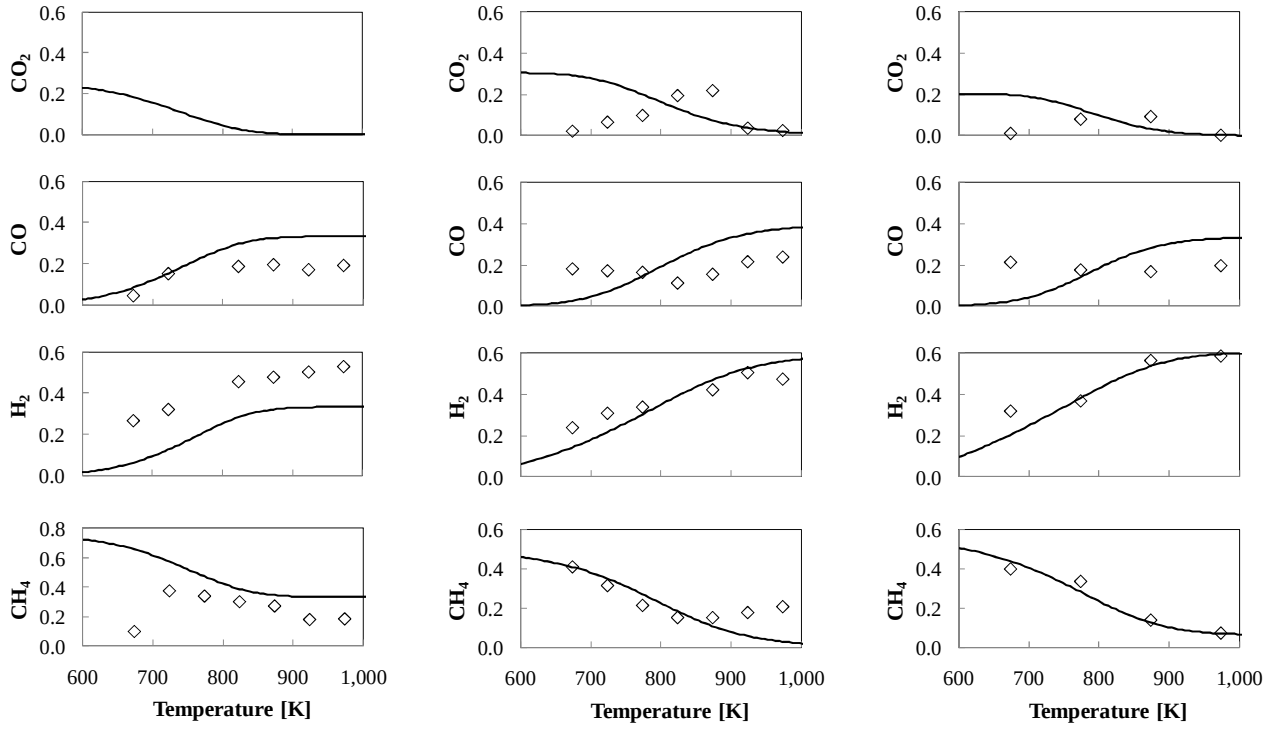

Figure 5. Gas phase mole fraction of the main species from (a) TD, (b) POX and (c) SR of ethanol on Ni/NASF catalyst. Continuous lines represent the mole fractions at thermodynamic equilibrium. Experimental conditions are presented in the Table 1.

4. CONCLUSIONS

Here, the thermal decomposition, partial oxidation and steam reforming of ethanol over SiO_2 supported Ni was studied in a packed bed reactor in the 673 - 973 K temperature range at 1 atm. The catalyst was produced from 10% NiO, 5% of bentonite and 85% (wt.) of natural amorphous silica fibers (NASF). Scanning Electron Microscopy evaluation revealed that Ni particles were homogeneously distributed over the NASF. The TD of ethanol occurs mainly by the dehydrogenation reaction generating acetaldehyde. Further, CH_3CHO is decomposed to CH_4 and CO. In parallel to this route, ethanol is dehydrated producing ethylene, which is successively dehydrogenated in Ni sites generating carbon on the surface. Also, carbon can be produced by consecutive dehydrogenation of CH_4. Both reactions contribute to increase the production of H_2 to values higher than those predicted by the thermodynamic equilibrium. Since CH_4 is almost equilibrated in studied temperature range, a lower catalyst deactivation of the POX and SR reaction is expected.

5. REFERENCES

Alcalá, R., Mavrikakis, M., Dumesic, J.A., (2003), “DFT studies for cleavage of C–C and C–O bonds in surface species derived from ethanol on Pt(111)” Journal of Catalysis 218 178–190.

Alexander Burcat and Branko Ruscic, (2005) "Third Millennium Ideal Gas and Condensed Phase Thermochemical Database for Combustion with updates from Active Thermochemical Tables" ANL-05/20 and TAE 960 Technion-IIT, Aerospace Engineering, and Argonne National Laboratory, Chemistry Division.

Donadel, K., (2010), "Synthesis and characterization of catalytic filters for combustion systems", Ph.D. Thesis (in Portuguese), Federal University of Santa Catarina.

Liberatori, J.W.C., Ribeiro, R.U., Zanchet, D., Noronha, F.B., Bueno, J.M.C., (2007), “Steam reforming of ethanol on supported nickel catalysts”, Applied Catalysis A: General 327, 197–204.

Lima, S.M., Cruz, I.O., Jacobs, G., Davis, B.H., Mattos, L.V., Noronha, F.B., (2008), “Steam reforming, partial oxidation and oxidative steam reforming of ethanol over $Pt/CeZrO_2$ catalyst”, Journal of Catalysis 257, 356–368.

Marinov, N., (1999), "A detailed chemical kinetic model for high temperature ethanol oxidation", International Journal of Chemical Kinetics 31, 183-220.

Mavrikakis, M., Barteau, M.A., (1998), “Oxygenate reaction pathways on transition metal surfaces”, Journal of Molecular Catalysis A: Chemical 131, 135–147.

Reynolds, W.C., (1986), "The element potential method for chemical equilibrium analysis: Implementation in the interactive program STANJAN 3", Stanford University.

S.M. Gates, J.N. Russell Jr., J.T. Yates Jr., (1986), "Bond Activation sequence observed in the chemisorption and surface reaction of ethanol on Ni(111)", Surface Science 171, 111-134.

Silva, A.M., Costa, L.O.O., Barandas, A.P.M.G., Borges, L.E.P., Mattos, L.V., Noronha, F.B., (2008), "Effect of the metal nature on the reaction mechanism of the partial oxidation of ethanol over CeO_2-supported Pt and Rh catalysts", Catalysis Today 133–135, 755–761.

Vesselli, E., Coslovich, G., Comelli, G., Rosei, R., (2005), "Modelling of ethanol decomposition on Pt(111): a comparison with experiment and density functional theory", J. Phys.: Condens. Matter 17, 6139–6148

Wang, G., Wang, H., Tang, Z., Li, W., Bai, J., (2009), "Simultaneous production of hydrogen and multi-walled carbon nanotubes by ethanol decomposition over Ni/Al_2O_3 catalysts", Applied Catalysis B: Environmental 88, 142–151.

6. ACKNOWLEDGEMENTS

This work was developed within the framework of projects - Edital MCT/CNPq 02/2006 – Universal (Processo: 485803/2006-2) and Edital MCT/CNPq Nº 014/2008 – Universal (Processo: 471062/2008-1). The authors also acknowledge the CNPq for the scholarships for R.C. Catapan and K. Donadel.

7. RESPONSIBILITY NOTICE

The authors are the only responsible for the printed material included in this paper.